The Influence of Salts on the Detection of Organics from Ocean Worlds via Laser Desorption Mass Spectrometry

Meridian McCall
GEOL 394 Final Report
November 25, 2024
Advisors: Dr. Ricardo Arevalo Jr., Madeline Raith, Lucas Andrews

Abstract

Over a decade ago, NASA's Cassini spacecraft discovered volatile-rich and organic-bearing ice particles erupting from the subsurface ocean of Enceladus. Since then, Enceladus has attracted significant interest from the astrobiological community due to the discovery of particles containing aromatic carbon structures, such as benzene (C_6H_6), and volatiles like hydrogen, methane, and ammonia. Further analysis by NASA's Cosmic Dust Analyzer classified the collected particles into three categories, with Types II and III being crucial for this study. Type II particles contain volatiles and organic compounds of high molecular weight (43-80 u), (Waite et al., 2006 and Postberg et al., 2018), and Type III, which consists of salt-rich particles (Postberg et al., 2023). These particles coexist in Saturn's orbiting E-ring, but the limits of detecting organics within salt-rich particles in situ remain uncertain.

This investigation will use Laser Desorption Mass Spectrometry (LDMS), a spatially resolved analytical technique capable of identifying organic molecules with geological context (e.g., host phase), to investigate how the salts observed in Type III particles from Enceladus inhibit or enhance the detection of refractory organic molecules. Here, we explore the limits of detection for multiple classes of organic compounds, such as amino acids (histidine and tryptophan) and nucleotides (adenine and thymine), in salt-rich water samples that serve as analogs to materials derived from the Enceladus plume. These specific organics and their relative abundances serve as prospective biosignatures in the search for extraterrestrial life (Neveu et al., 2018) (Neveu et al., 2020). Three distinct salt solutions consisting of NaCl, $NaHCO_3$, and Na_3PO_4 will act as proxies for dissolved salts in the Enceladus subsurface ocean. Each salt solution is doped with 12 concentrations of organics spanning six orders of magnitude (1 mM to 3 nM). Aliquots of each solution are applied to a stainless-steel plate and allowed to evaporate, simulating the sublimation of Enceladus plume materials and leaving behind a salt and organic-rich residue. The dried residue is analyzed via LDMS, and the data collected is used to construct a calibration curve based on the average signal-to-noise ratio (S/N). The limit of detection of each organic compound interpolated from these curves enables comparative analysis of the effect of the salty matrices. The results will inform whether the specific salt measurably influences LDMS detection limits for the organic analytes investigated in each sample. Overall, this study will ultimately help define the performance requirements for future LDMS payload instruments when used quantitatively.

Plain Language Summary

Saturn's moon, Enceladus, has sparked tremendous interest within the astrobiological community because it meets all the criteria thought to be required for the emergence of life. NASA's Cassini spacecraft collected particles ejected from Enceladus' subsurface ocean and discovered key chemical constituents such as water, gas, salts, and organic molecules consisting of carbon, hydrogen, oxygen, nitrogen, and phosphorus (CHONP). Sampling of these particles revealed a salty and organic-rich ocean beneath the icy crust of Enceladus. This study focuses on how future detection of amino acids (building blocks of proteins) and nucleobases (building blocks of RNA and DNA) might be challenged by the presence of mineralogy, i.e., salts found on Enceladus. These organics may serve as important markers of life due to their vital roles in the fundamental processes of cellular function and genetic information storage. Three salts are selected to simulate the observed molecular composition ejected from the Enceladus plume. The salts will be used to create a series of solutions that will be doped with a combination of organics with varying

concentrations. After the organics dissolve, the solutions will be left to evaporate. The residue will be loaded into a commercial instrument that analyzes the chemistry of solid materials using a laser and mass spectrometer, allowing the detection limits of organics in the remaining salts to be quantified.

Introduction

Nationally recognized as a high-priority astrobiology target in the most recent Planetary Science Decadal Survey, Enceladus provides promising evidence for the search for life beyond Earth (National Academies of Sciences et al., 2023). Imaging from NASA's James Webb Space Telescope's Near-Infrared Spectrograph depicts a water vapor plume spewing material from the southern region of Enceladus, corroborating original observations made by Cassini (via X-ray, ultraviolet, and infrared imaging) decades earlier. Together, these findings suggest sustained activity in the moon's southern hemisphere, indicating a continuous source of material being ejected from beneath the icy surface. These observations prompted NASA to deploy its Cassini spacecraft, which, during its first flyby in February 2005, returned data supporting speculations about vapor plume emissions composed of icy particles (Waite et al., 2006).

Successive flybys of Enceladus revealed other in situ analyses of emitted grains, as enabled by the Cassini Cosmic Dust Analyzer (CDA), to provide unique information about the subsurface ocean's composition. The CDA recorded thousands of time-of-flight mass spectra of ice particles through impact ionization. It provided direct observations of dust grains, including data on their mass and composition, by analyzing the ions produced on detector surface via mass spectrometry (Srama et al., 2004). From the detected particles, which exhibited radii of 0.1-1 mm (Srama et al., 2004), there appeared to be distinct families of spectra, classified as Types I, II, and III, based on the relative abundances of specific molecules. Type I particles are composed almost entirely of pure water ice, while Type II particles contain significant amounts of organics and/or siliceous material (Fig. 1) (Srama et al., 2004). Type III particles exhibit a mass line pattern characterized by distinct peaks in a spectrum, which correspond to their high sodium content (Fig. 2) (Postberg et al., 2009). Type II particles collected from the CDA have uncovered simple compounds consisting of C, H, O, N, and P (Postberg et al., 2009, 2023), providing supporting evidence for the potential habitability of the subsurface environment (Wasson et al., 1988). Samples containing nitrogen in the form of NH_3 and HCN are known chemical precursors of amino acids and many other complex organic compounds (Neveu et al., 2020). 11/26/2024 1:07:00 AMAdditionally, Type III particle peaks indicate that sodium salts, such as NaCl, $NaHCO_3$, and Na_2CO_3, are major constituents with weaker K^+ peaks, which suggests a minor contribution to this population of particles (Postberg et al., 2009). Phosphorus also appears sodiated within Type III spectra particles (Postberg et al., 2023). Thus, five of the six major elements key to life on Earth ("CHNOPS") have been detected in ocean-derived material from Enceladus.

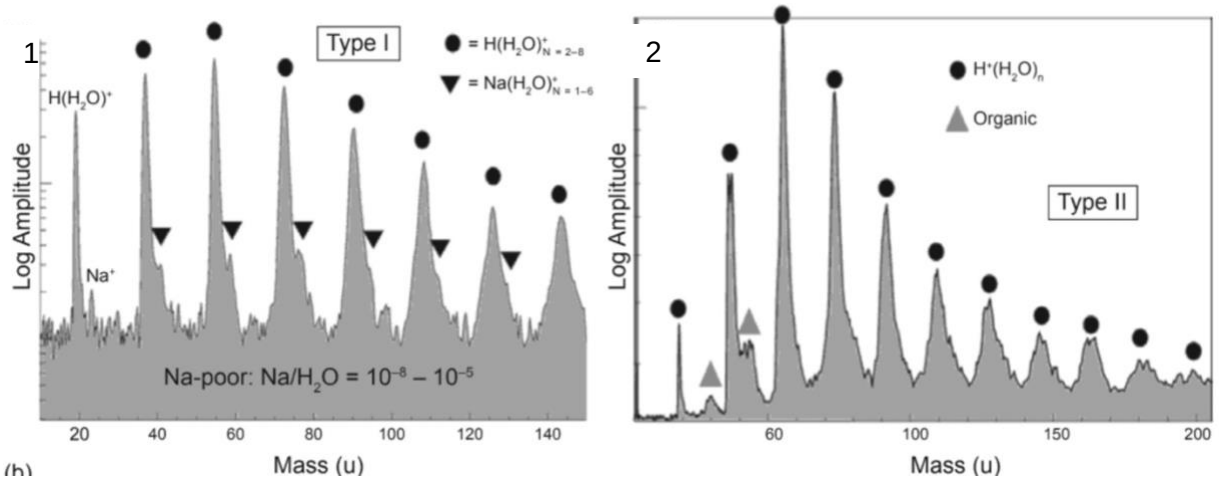

Figure 1. :(Postberg et al., 2009)
Spectra of water-ice particles (Type I), and (Type II) spectra of water ice with high abundance of organics. Peak masses can be identified by the black circles [p^+] H_20 and grey triangles, which represents relatively high mass organics.

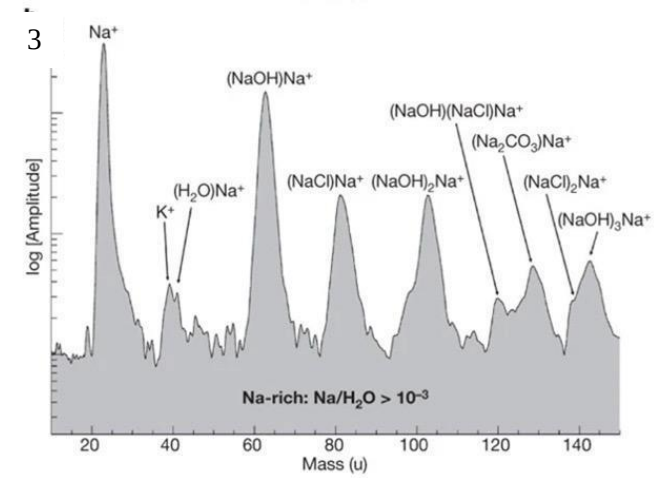

Figure 2. : (Postberg et al., 2009)
Spectra of Na-rich water-ice particles (type III). Although particles are predominantly water, these spectra have Na-hydrate clusters. They are characterized by an abundant Na^+ mass line followed by a sequence of peaks from hydroxyl-cluster-ions, representing Type III spectrum.

As the only ocean world deemed top priority for Flagship mission type, NASA plans to further investigate the nature of Enceladus's plume activity, including the physical conditions and chemistry of the source. Studying these features can help uncover prevailing and/or the early emergence of biological activity. These investigations will contribute to developing an understanding of the habitability of oceans beyond our remote observations from Earth. Considering these objectives, a pivotal focus lies in the search for biosignatures within Enceladus's plume and, by extension, subsurface ocean. Here, the term biosignature is defined as "any phenomenon for which biological processes are a known possible explanation and whose potential abiotic causes have been reasonably explored and ruled out." Although abiotic processes can form prebiotic molecules like amino acids and even nucleobases (Cafferty & Hud, 2014; Guo et al.,

2023; Tolstoguzov, 2004), as confirmed by the organic inventory of meteorites (Cobb & Pudritz, 2014). With the ingredients of nitrogen and oxygen-bearing compounds known as amines and carbonyls, as well as compounds with ring-shaped molecular structures – known as aromatic compounds – available in the Enceladus Ocean (Postberg et al., 2018), the accessibility of the components needed to polymerize larger molecules like amino acids and nucleobases (and ultimately proteins and DNA/RNA, respectively) underscores their significance as biological signatures. However, it is also important to emphasize that without biological interference, it is more likely that these molecules will remain merely pieces of a larger puzzle.

The objective of this study is to investigate whether salt mineralogy influences the detectability of organic material analyzed via LDMS techniques. The ability to detect organics in salt-rich matrices on Enceladus is strongly dependent on the substrate's properties. In the presence of monovalent cations (e.g., Na^+), compounds with multi-ringed structures (e.g., adenine) are preferentially adsorbed over molecules with fewer aromatic rings (e.g., thymine), as demonstrated by (Franchi, 2003).“Chloride salts, such as NaCl and KCl, are critical planetary materials due to their ability to depress the freezing point of liquid water in cryogenic environments and to concentrate dilute organic monomers through adsorption onto mineral surfaces”, (Arevalo et al., 2023). Salt-rich substrates play a significant role in geochemical and biochemical processes on ocean worlds like Enceladus, where geological context may influence the LOD for organic biosignatures.

Three salt solutions consisting of NaCl, $NaHCO_3$, and Na_3PO_4 and four organic compounds were selected to serve as putative biosignatures. The first two analytes, histidine ($C_6H_9N_3O_2$) and tryptophan ($C_{11}H_{12}N_2O_2$), are essential amino acids that act as the building blocks of peptides and proteins in terrestrial life. The second pair of analytes, adenine ($C_5H_5N_5$) and thymine ($C_5H_6N_2O$) represent nucleobases, monomers of genetic material (e.g., DNA/RNA). The salt solutions were doped with varying concentrations of all four organic compounds. In considering the absence of a significant effect or relationship, the null hypothesis states that salt composition will not impact the detection limit of the organic analytes, as measured by LDMS. This study aims to ascertain whether salts derived from the Enceladus subsurface ocean will promote or inhibit the detection of biosignatures using LDMS, a technique compatible with spaceflight applications, thereby informing multiple mission concept studies.

Methods

LDMS serves as a powerful tool for detecting organic molecules and inorganic elements simultaneously. The technique involves ablating and ionizing a sample surface (typically a solid) using a pulsed laser. Ions are sorted according to their respective mass-to-charge ratios and detected by an Orbitrap™ mass analyzer that offers ultrahigh mass resolving powers and mass accuracies (Scigelova et al., 2006). More abundant ions will be observed at higher signal intensities than lower abundance ions. By normalizing analyte concentrations and intensities, LDMS has the capability to quantify compounds such as amino acids more effectively (Alterman et al., 2004).

The organic analytes targeted in this investigation are of intermediate fidelity as biosignatures. Bodies like meteorites are known for having abundances of amino acids, some of which are unlike the specific terrestrial amino acids we see here on Earth. Abiotic mechanisms of synthesis are unable to synthesize late amino acids (appearing later in evolutionary history), which are essential

to genetic code (Higgs et al., 2009). However, simpler amino acids are more common and easily synthesized on the surfaces of chondrites (Cobb et al., 2014)). The chosen amino acids under analysis, histidine, and tryptophan serve as higher fidelity biosignature for this study since they are observed less in spontaneous synthesizing environments, they are also terrestrial compounds linked to life on Earth. Histidine specifically is not found abiotically (Neveu et al., 2020). The complexity of amino acids varies between those formed through abiotic processes, which predominantly produce simpler compounds like glycine, and those generated biotically, which are typically more complex, such as histidine and tryptophan (Creamer et al., 2017; McKay, 2004).

Nucleobases, which serve as the precursors of genetic material, are also utilized in this study to represent biosignatures. Adenine and thymine pair with other bases to form what is recognized as DNA and RNA. Indications of these molecules in the search for biological signals would demonstrate a plausible link to the dispersions of life concurrent with that on Earth. Most of all known terrestrial life uses DNA as its genetic material. The detection of nucleic acid biosignatures such as adenine and thymine in extraterrestrial environments might imply the existence of organisms like those found on Earth (Mojarro et al., 2017). While adenine and thymine have been observed on meteorites, no nucleobase has been found to date in interstellar space (Jiménez-Serra et al., 2020; Snyder et al., 2005). However, "only eight nucleobases indigenous to meteorites have been detected to date, compared to the 96 different amino acids that have been identified", (Martins et al., 2018). The presence of nucleobases in extraterrestrial environments supports plausible existence of life beyond Earth.

The detection limits of all four molecules in a salty residue were analyzed via LDMS. The limits of detection are typically expressed in terms of the minimum concentration of the analyte that can be detected at or above S/N =2. In the context of the LDMS instrumentation, "noise" refers to unwanted or random fluctuations in a signal that can interfere with the accurate detection and measurement of the desired signal. Here, the S/N is calculated by dividing the height of individual ion peaks by the level of noise (present at the base of the peaks).

Three salts, specifically sodium chloride (NaCl, sodium bicarbonate ($NaHCO_3$), and sodium phosphate (Na_2PO_4), were selected with the intent to simulate the molecular composition observed in the Enceladus Type III plume particles (Table. 1). The three salts, sodium chloride (NaCl), sodium bicarbonate ($NaHCO_3$), and sodium phosphate (Na_2PO_4), were prepared in 150 ml of solution at 0.1 M. The necessary weight in grams for the organic stock solution was weighed to make 100 ml of solution at 0.003 M, the molecular weight of organics reported in Table 2. The mixture of organics was added to the salt solution and agitated using a sonicator to fully dissolve the contents of the organics. Once fully dissolved, a dilution series of 12 concentrations was performed, containing about 33.3% organic in each solution. The first concentration, 1 mM, followed by 310 uM and decreases, as described in Table 3. 2 uL aliquots of the sample were transferred to an organic-free stainless-steel plate by pipette. The stainless-steel plates were thoroughly cleaned through sonication using a sequential cleaning protocol: acetone, isopropanol (IPA), methanol, acetone (repeated), and finally deionized water. Three aliquots of each solution were deposited onto different regions of the plate to assess external reproducibility. Dried samples were labeled with their corresponding concentrations. A blank containing just the salt solution was included for each plate.

Once fully dry, the samples were loaded into the sub-atmospheric pressure chamber of a Thermo Scientific Q Exactive Orbitrap Mass Spectrometer equipped with a custom pulsed laser source and sample chamber designed and installed by Spectroglyph, LLC. All analyses scanned across a mass range of 50 - 750 m/z, detecting positive ions with a mass resolving power of $m/\Delta m = 70{,}000$ (FWHM at m/z 400). LDMS data were processed using Freestyle, a Thermo application used to view and analyze raw mass spectrometry data. Freestyle uses the original intensity versus frequency data from the mass spectrometer, sorts by frequency intervals, and then uses the instrument's mass calibration file to convert the frequency data to m/z values. (*Freestyle User Guide*, 2021). This program outputs the average intensity and (S/N) across ~ 150 scans. In the FreeStyle software, a default (S/N) ratio threshold of 2.0 is applied as a criterion for peak detection. This means that chromatogram peaks with S/N values below 2.0 are ignored during analysis unless adjusted to another parameter (*Freestyle User Guide*, 2021). The (S/N) ratios from nine analyses at each concentration were averaged and plotted on a calibration curve in Excel to visualize the detected organic compounds as peaks corresponding to their respective concentrations.

Salts	Observed concentration abundance
Sodium Chloride (NaCl)	0.05-0.2 mol kg -1
Sodium Bicarbonate ($NaHCO_3$)	0.02-0.1 mol kg -1
Sodium Phosphate (Na_3PO_4)	10-7-10-2mol/l

[Table 1]: A summary of salts used within the study along with their corresponding molecular weights. Observed abundances from

Organic	Molar Mass (g)
Adenine $C_5H_5N_5$	135.13
Thymine $C_5H_6N_2O_2$	126.11
Histidine $C_6H_9N_3O_2$	155.15
Tryptophan $C_{11}H_{12}N_2O_2$	204.23

[Table 2]: A summary of chosen organics serving as biosignatures, along with their equivalent molecular weights.

Concentrations of Dilution Series of 0.1M
1mM
310 uM
100 uM
30 uM
10 uM
3 uM
1 uM
300 nM
100 nM
30 nM
10 nM
3 nM

[Table 3]: Dilution series concentrations for salt solutions.

Data

Fragment identification for the analyzed organics was achieved by comparing the detected m/z values from the doped samples to those of the blank samples. This comparison allowed for the isolation of organic fragments present only in the doped analysis. Common fragmentation patterns from the NIST Mass Spectrometry Data Center for ionized molecules, combined with computations of lost mass units, were used to identify the detected m/z values for each molecule. The peak m/z identified for thymine was 95.060, approximately 39.993 mass units away from its monoisotopic mass, indicating the loss of hydrogen, nitrogen, and oxygen atoms. For adenine, a peak at 136.062 was consistent with the monoisotopic mass of protonated adenine. A peak at 110.072 matched the monoisotopic mass of protonated histidine. Lastly, a peak at 130.064 was identified as a common fragment of tryptophan, representing a protonated molecule that had lost two carbons, two oxygens, one nitrogen, and four hydrogens. These values for adenine, histidine, and tryptophan showed a high confidence of identification, as the observed peaks closely aligned with expected fragmentation patterns. Calculations of mass accuracy up to the third significant figure (Actual Mass-Observed Mass) / (Actual Mass) ensured that all organics fell within a tolerance of 10 Δppm, indicating excellent agreement with theoretical values and supporting the fragment identification.

To evaluate the limits of detection (LOD) for organics in salt solutions, the dilution series spanning 12 concentrations of each organic compound was analyzed against the averaged (S/N) ratios. A linear best-fit regression was applied to the viable data points. Data were included up to the

concentration corresponding to the first negative detection, with exceptions made for anomalous measurements where no detection occurred between two positive detection points. The sensitivity curves for the various organics against salts, NaCl, $NaHCO_3$, and Na_3PO_4, can be observed in Figures 6-8. Supplemental error calculations for standard deviation (STDEV) of individual data points per salt are provided in the tables following the graphs. Additional figures (Figures X-V) represent the linear regression of organics versus the concentration of each salt analyzed via a Monte Carlo simulation to estimate the probability distribution of the true best-fit line. Monte Carlo simulations are particularly useful in assessing the impact of uncertainty and variability in models. Instead of relying on fixed input values, this method uses probability distributions to model the uncertainty for the Y-values. By recalculating results multiple times—1,000 iterations in this case, using an in-house MATLAB code—a wide range of potential best-fit lines can be generated, each informed by the specified bounds of the STDEV of organics. From the generated linear best-fit lines, the LOD was quantified using the slope-intercept formula. The mean of 1000 trials was averaged to quantify the LOD and STDEV displayed in the tables below.

Discussion

The limit of detection (LOD) for organic molecules was found to be highly sensitive to the salt matrix used for analysis. For tryptophan, the lowest LOD was observed in Na3PO4, followed by NaCl and $NaHCO_3$ (Tables 16 -18). This pattern repeats in the rest of the organics, adenine, thymine, and histidine. All achieved lower LOD in the sodium phosphate matrix making it the most effective for detecting these organics. NaCl also yielded competitive LOD values, often overlapping with Na_3PO_4 within the margin of error. Conversely, $NaHCO_3$ proved the least effective matrix, as organics frequently lacked significant signal at lower concentrations, resulting in higher LOD values. Among the analytes studied, tryptophan, histidine, and adenine were not only more detectable across all salt matrices, providing more data points, but also consistently showed lower LOD values than thymine in NaCl, $NaHCO_3$, and Na_3PO_4.

Nucleic acids, adenine, and thymine exhibit strong UV absorption due to their aromatic ring structures, which contain conjugated double bonds that interact effectively with UV light. Adenine, with its larger ring structure, absorbs UV light more intensely than thymine, which has a simpler ring structure (Tanaka & Nagakura, 1966). Tryptophan's side chain, composed of a benzene ring fused to a nitrogen-containing aromatic ring, also contains a conjugated double-bond system that facilitates electron transitions upon UV exposure, resulting in strong UV absorption and interaction with sodium ions (Antoine & Dugourd, 2013). Similarly, histidine's side chain, an aromatic five-membered ring with two nitrogen atoms, absorbs UV light less strongly than tryptophan (Permyakov, 2012) . Thus, it is not surprising that tryptophan and adenine achieved lower LODs than histidine and thymine, whose ring structures are less complex.

The observed differences in the LOD for organics when using various salt matrices (NaCl, Na_3PO_4, $NaHCO_3$) can be examined by considering the effects of properties such as UV absorption, thermal conductivity, and crystal structure of the matrices. A matrix with a high UV absorption can aid in ionizing the organics within the sample. NaCl has a UV absorption of 193-213 nm (Dair, 2001) . Na3PO4 has a comparable range with a 185-210 nm UV absorption (Halmann & Platzner, 1965). NaHCO3 has a UV absorption of 193.4 - 277.0 nm (Self & M. C. Plane, 2002). NaHCO3 had the highest range for its UV absorption but still had the highest LOD.

Thermal conductivity measures a material's ability to conduct heat. The higher the thermal conductivity, the more efficiently heat is transmitted throughout the material. NaCl thermal conductivity of 5.94 W/m K likely contributes to its lower LOD of organics (Keller, 2017). In contrast, the low thermal conductivities of Na_3PO_4, 0.7 W/m K, and $NaHCO_3$ 0.6 W/m K might result in less efficient ionization, particularly in NaHCO (Keller, 2017). Na_3PO_4 and $NaHCO_3$ have thermal conductivities that resist the flow of heat, possibly promoting some localized ionization but likely resulting in uneven energy distribution. This may explain why $NaHCO_3$ shows the highest LOD despite having a broader UV absorption range. This, however, does not explain why sodium phosphate outperformed NaCl as the analyte's matrix.

Crystal structure may also play a significant role in the effectiveness of the salt matrix. The crystal lattice of these sodium matrices may influence ionization efficiency, referring to how well the neutral molecules in a sample are converted into gas-phase ions during the laser desorption process. NaCl's cubic crystal structure, with three equal axes, all perpendicular, creates a simple and symmetrical surface that could potentially promote analyte ionization. Na_3PO_4's orthorhombic structure, characterized by three mutually perpendicular axes of different lengths, might create an irregular surface, altering ionization depending on the location of the laser shot on the surface. Surfaces where phosphate groups are closely packed and sodium ions are fully coordinated are likely less reactive. Higher energy planes, due to fewer bonds, are more reactive because they are less stable (Mavrikakis et al., 1998). $NaHCO_3$'s monoclinic structure, with three unequal axes and only two perpendicular axes, likely produces the most irregular surface, potentially scattering laser energy and reducing analyte ionization efficiency.

These properties alone are not enough to definitively explain why sodium phosphate outperforms its counterpart matrices. From the analysis of the three properties discussed above, it is possible that the organics favor the Na_3PO_4 crystal surfaces, potentially due to the reactivity of specific planes or interactions unique to its orthorhombic structure. Alternatively, the outcome could result from a combination of all three factors—UV absorption, thermal conductivity, and crystal structure—acting together in ways not fully understood within the scope of this study. This remains an area for further exploration.

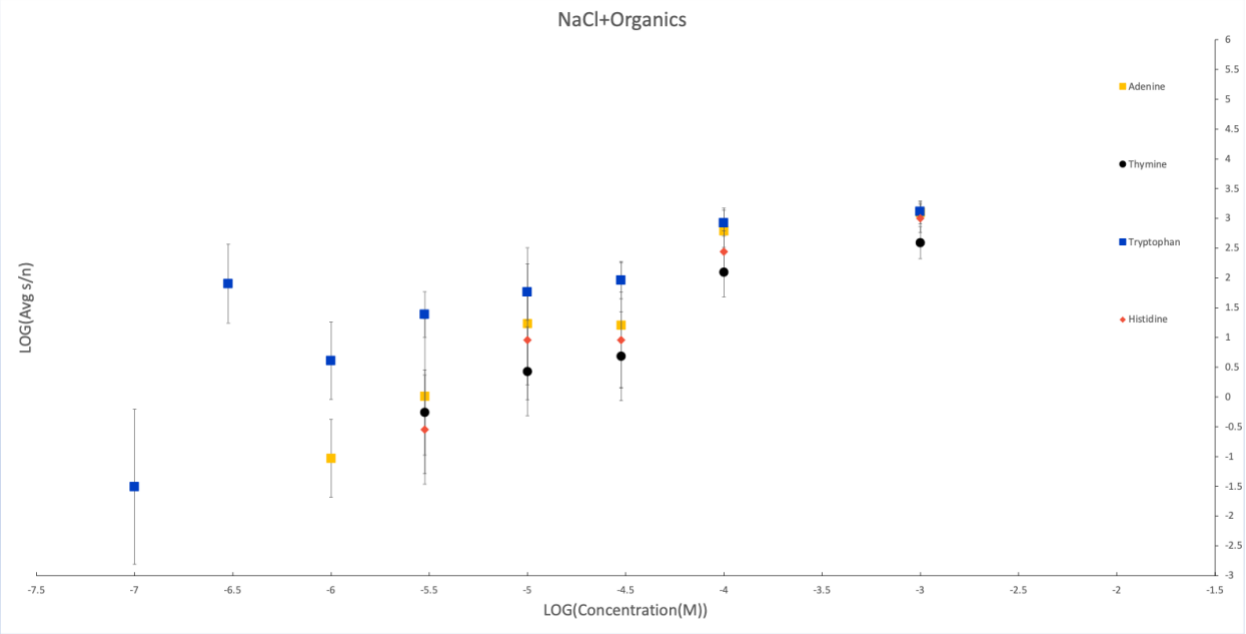

Figure 6: A sensitivity curve of the identified peaks within the NaCl sample. Each colored plot represents a different peak displaying a specific mass number along varying concentrations in the log scale. The yellow squares represent protonated adenine ($[M+H]^+$), the black circles a common fragment of thymine ($C_5H_6N_2O_2$), the red diamonds protonated histidine, and the blue squares a fragment of tryptophan ($C_{11}H_{12}N_2O_2$).

Avg(S/N)- Tryptophan (NaCl)	STDEV
1313.4456	0.346366
0.1275	1.62409
836.70222	0.507517
92.043333	0.7251
58.052222	1.080328
24.331111	0.886229
4.0755556	1.494356
79.803333	1.527295
0.0311111	3
0.1466667	1.280566
0	-
0	-

[Table 4]: A summary of STDEV, from averaged Tryptophan (S/N).

Avg(S/N)- Histidine (NaCl)	STDEV
996.6433	0.546845
0	-
275.5478	0.812459
9.09	1.851966
9.018889	1.726675
0.283333	2.1091
0.067778	1.52578
0.037778	2.189942
0.153333	1.664961
0.02	3
0	-
0	-

[Table 5]: A summary of STDEV, averaged Histidine (S/N).

Avg(S/N)- Adenine (NaCl)	STDEV
1251.43	0.440905
0	-
613.8778	0.8879035
16.10778	2.4089833
17.07778	2.9420418
1.035556	3
0.093333	1.5028672
0.224444	1.0303335
6.077778	1.9173554
0	-
0	-
0	-

[Table 6]: A summary of STDEV, from averaged Adenine (S/N).

Avg(S/N)- Thymine (NaCl)	STDEV
391.80333	0.62773
0.0177778	3
125.73889	0.959744
4.85	1.716465
2.6833333	1.71348
0.55	1.651396
0.0211111	3
0	-
0.0277778	3
0.0211111	3
0	-
0	-

[Table 7]: A summary of STDEV, from averaged Thymine (S/N).

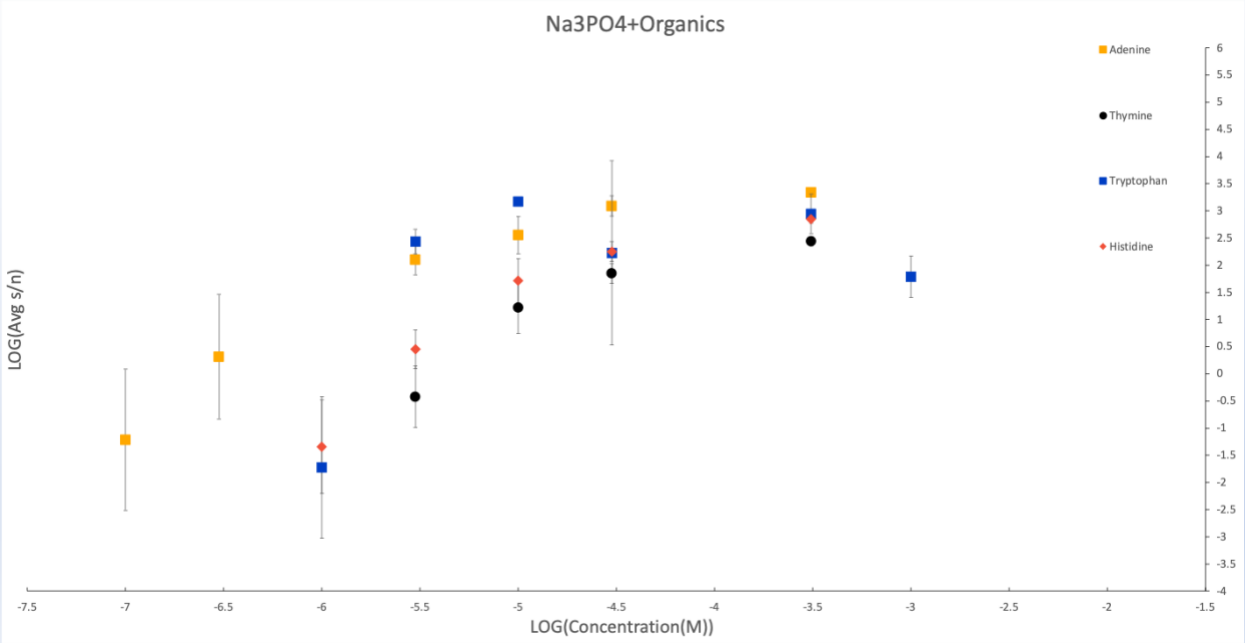

Figure 7: A sensitivity curve of the identified peaks within the Na_3PO_4 sample. Each colored plot represents a different peak displaying a specific mass number along varying concentrations in the log scale. The yellow squares represent protonated adenine ($[M+H]^+$), the black circles a common fragment of thymine ($C_5H_6N_2O_2$), the red diamonds protonated histidine, and the blue squares a fragment of tryptophan ($C_{11}H_{12}N_2O_2$).

Avg(S/N)- Tryptophan (Na_3PO_4)	STDEV
61.4966667	0.87091186
881.222222	0.84668737
0	-
169.208889	3.90238806
1485.67556	0.00313501
272.615556	0.51734734
0.01888889	3
1.44444444	1.15947646
6.15555556	1.15135676
14.1311111	1.57248681
0.07555556	1.55917033
0.04444444	1.9875

[Table 8]: A summary of STDEV, from averaged Tryptophan (S/N).

Avg(S/N)- Histidine (Na_3PO_4)	STDEV
0.02444444	3
702.333333	0.1578652
0.02	3
178.123333	0.42024572
52.0322222	0.93429504
2.83	0.81676288
0.04555556	1.98507219
0.06666667	2.14898232
0.04555556	1.99113144
0	-
0	-
0	-

[Table 9]: A summary of STDEV, from averaged Histidine (S/N)

Avg(S/N)- Adenine (Na_3PO_4)	STDEV
2.38666667	0.91691593
2173.98444	0.04728679
0	-
1227.34333	0.42626944
357.29	0.78831011
125.626667	0.63912509
0	-
2.06666667	2.6388286
0.06111111	3
20.6922222	1.64281338
14.98375	1.8505315
0	-

[Table 10]: A summary of STDEV, from averaged Adenine (S/N).

Avg(S/N)- Thymine (Na_3PO_4)	STDEV
0	-
273.92	0.20020088
0.02333333	3
70.27	0.41977274
16.6122222	1.0957514
0.37777778	1.30384629
0.02555556	3
0	-
0	-
0	-
0	-
0	-

[Table 11]: A summary of STDEV, from averaged Thymine (S/N).

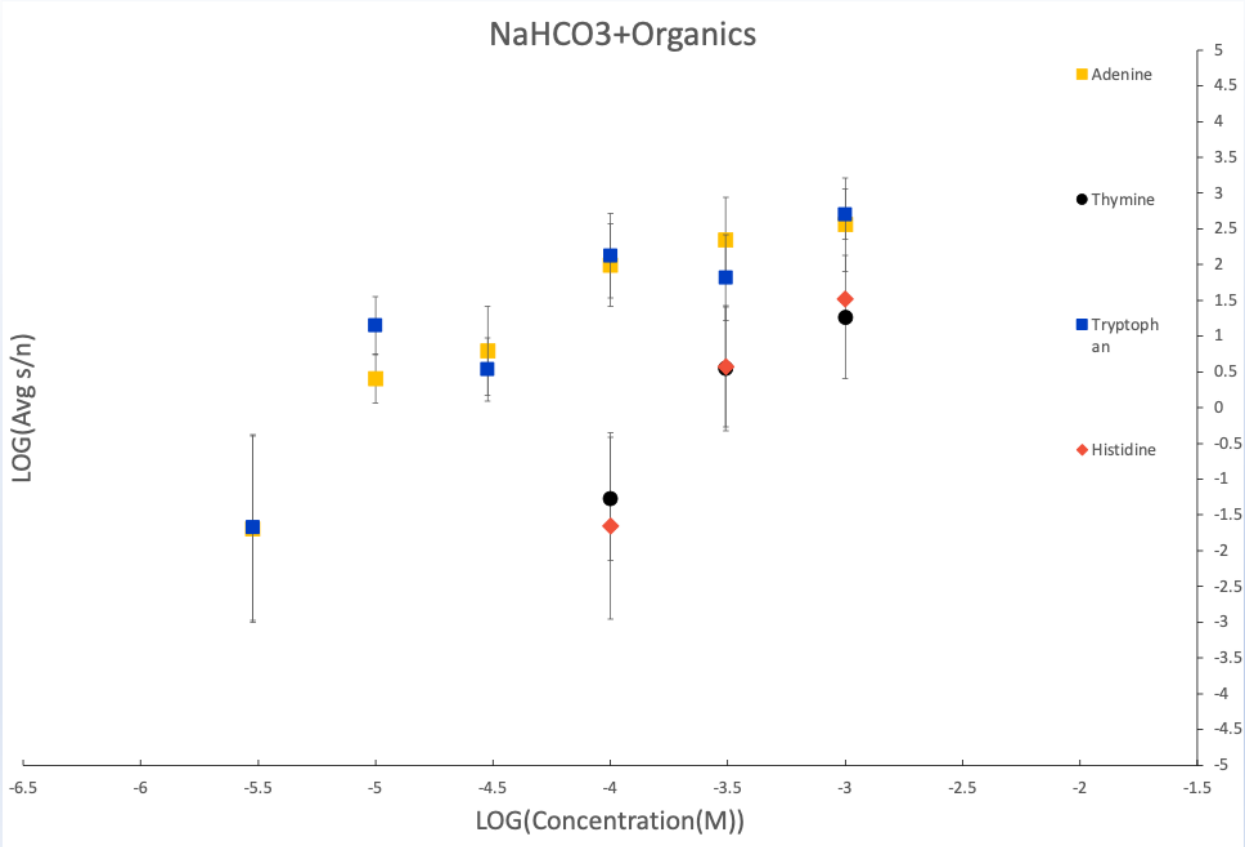

Figure 8: A sensitivity curve of the identified peaks within the $NaHCO_3$ sample. Each colored plot represents a different peak displaying a specific mass number along varying concentrations in the log scale. The yellow squares represent protonated adenine ($[M+H]^+$), the black circles a common fragment of thymine ($C_5H_6N_2O_2$), the red diamonds protonated histidine, and the blue squares a fragment of tryptophan ($C_{11}H_{12}N_2O_2$).

Avg(S/N)- Tryptophan ($NaHCO_3$)	SEM
508.4122	0.802791989
65.87778	1.375139158
132.56	1.357300634
3.427778	1.013143116
14.00444	0.927737474
0.021111	3
7.346667	1.526086838
0.017778	3
0.118889	1.97638694
0.096667	1.134398907
0.021111	3
0.245556	1.671806398

[Table 12]: A summary of STDEV, from averaged Thymine (S/N).

Avg(S/N)- Histidine ($NaHCO_3$)	STDEV
32.91444	0.002416
3.73	1.936165
0.022222	3
0	-
0.057778	1.505813
0	-
0	-
0	-
0	-
0	-
0	-
0.024444	3

[Table 13]: A summary of STDEV, from averaged Histidine (S/N).

Avg(S/N)- Adenine ($NaHCO_3$)	STDEV
362.7977778	1.506571
221.2666667	1.382369
98.73111111	1.335222
6.205555556	1.430897
2.532222222	0.791092
0.02	3
0.022222222	3
0	-
0	-
0	-
0.036666667	3
0.018888889	3

[Table 14]: A summary of STDEV, SEM from averaged Adenine (S/N).

Avg(S/N)- Thymine ($NaHCO_3$)	STDEV
18.39555556	1.985733503
3.54625	2.021575063
0.053333333	1.986526884
0	-
0	-
0	-
0	-
0	-
0	-
0.01	3
0	-
0	-

[Table 15]: A summary of STDEV, from averaged Thymine (S/N).

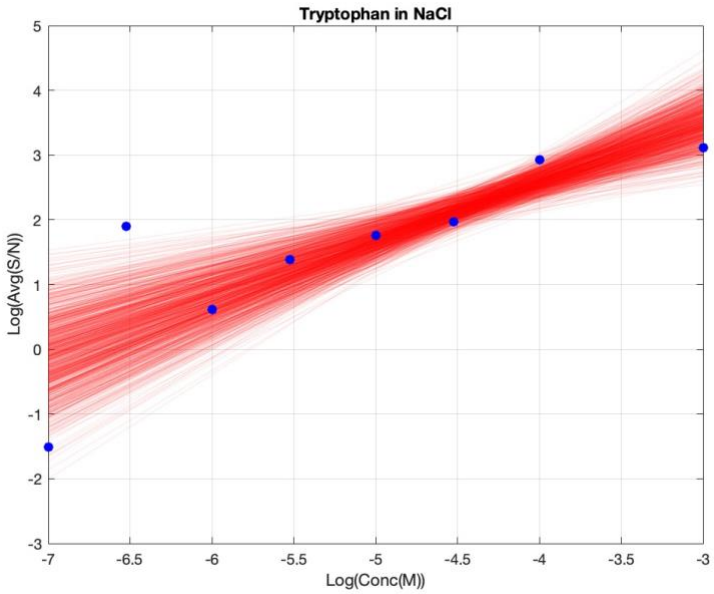

Figure 9: The Monte Carlo regression series, spanning 1000 iterations of the likely best fit according to STDEV of individual data points of tryptophan.

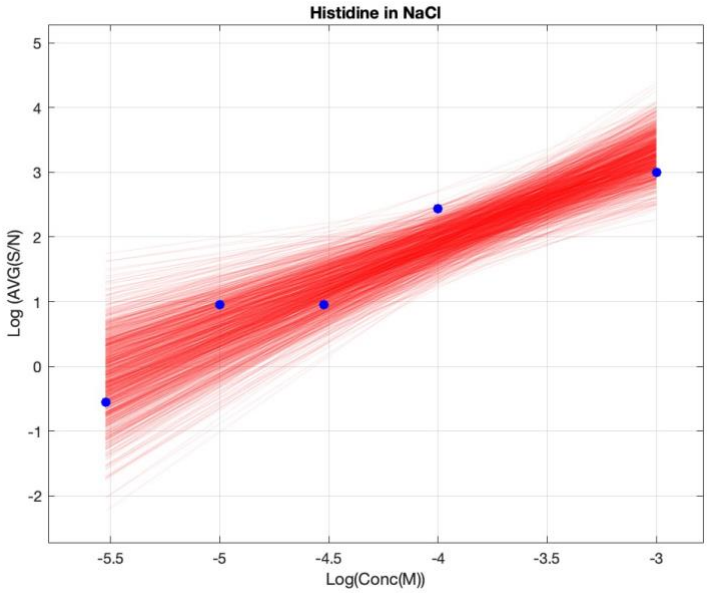

Figure 10: The Monte Carlo regression series, spanning 1000 iterations of the likely best fit according to STDEV of individual data points of histidine.

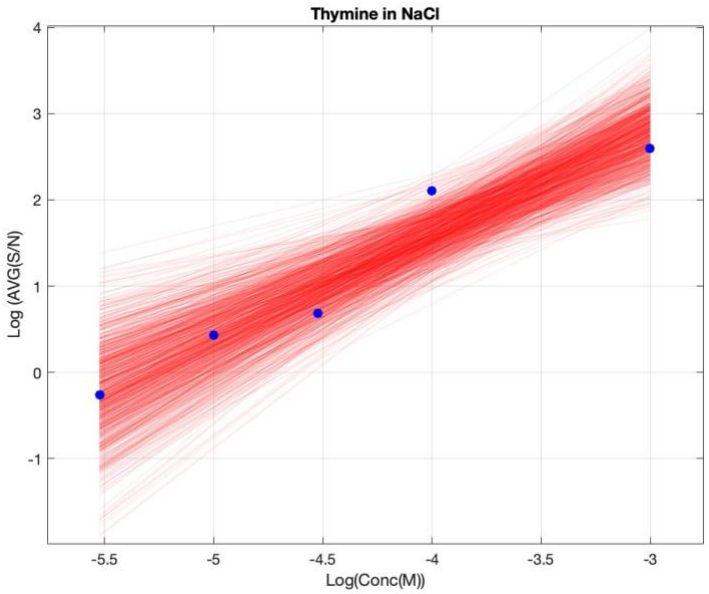

Figure 10: The Monte Carlo regression series, spanning 1000 iterations of the likely best fit according to STDEV of individual data points of thymine.

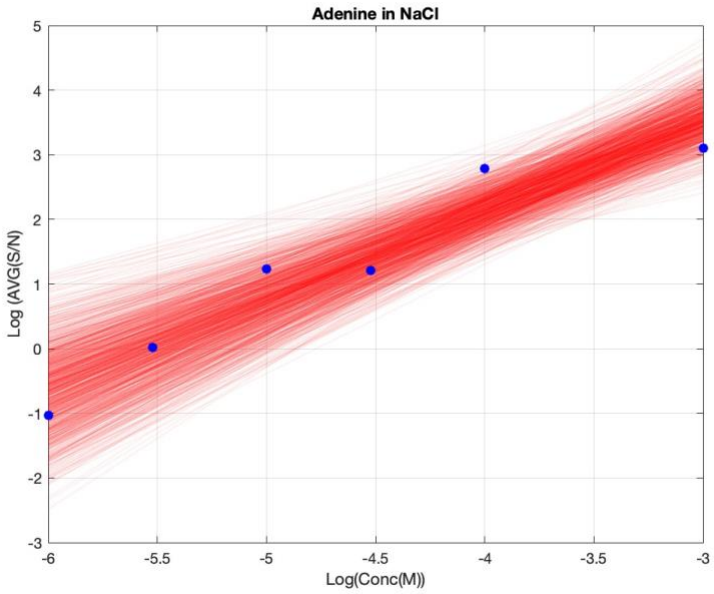

Figure 11: The Monte Carlo regression series, spanning 1000 iterations of the likely best fit according to STDEV of individual data points of adenine.

	Tryptophan	Histidine	Adenine	Thymine
LOD NaCl (M)	5.87412E-07	1.09765E-05	7.85396E-06	1.51755E-05
STDEV	3.779714593	2.328792368	2.234598102	2.1743294

[Table 16]: A summary of the LOD of organics in NaCl in M. The subsequent STDEV of the averaged 1000 trials is also listed. LOD of all organics falls within the order of magnitude of the averaged detection limit.

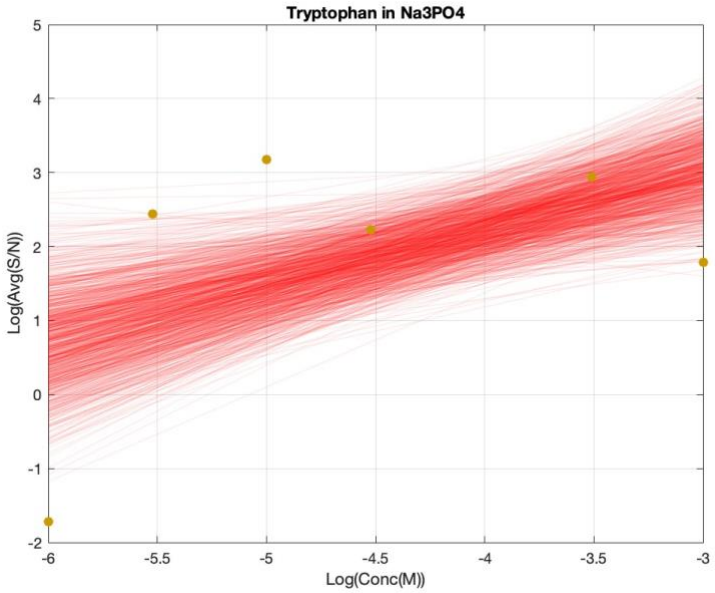

Figure 12: The Monte Carlo regression series, spanning 1000 iterations of the likely best fit according to STDEV of individual data points of tryptophan in sodium phosphate.

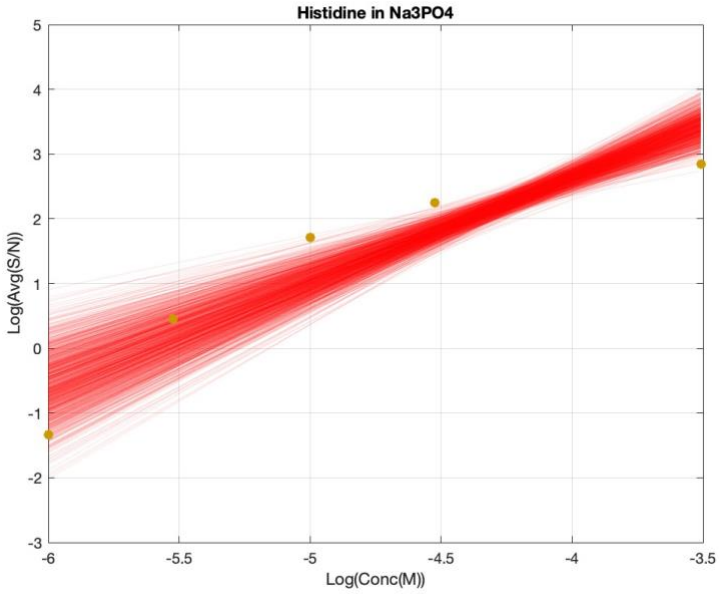

Figure 13: The Monte Carlo regression series, spanning 1000 iterations of the likely best fit according to STDEV of individual data points of histidine in sodium phosphate.

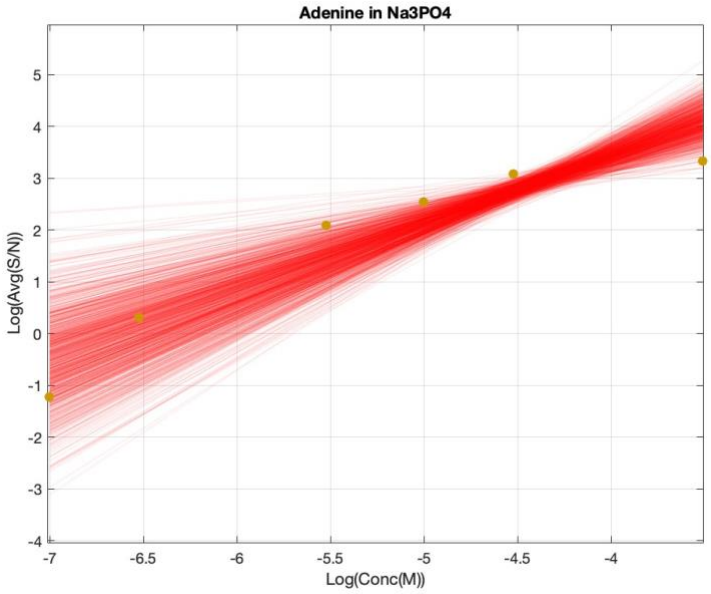

Figure 14: The Monte Carlo regression series, spanning 1000 iterations of the likely best fit according to STDEV of individual data points of adenine in sodium phosphate.

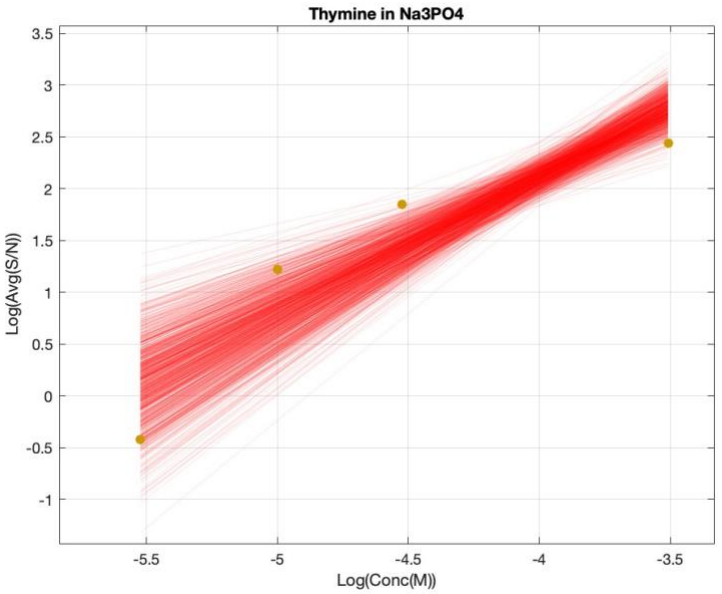

Figure 13: The Monte Carlo regression series, spanning 1000 iterations of the likely best fit according to STDEV of individual data points of thymine in sodium phosphate.

	Tryptophan	Histidine	Adenine	Thymine
LOD Na_3PO_4	2.22904E-07	5.67614E-06	5.83071E-07	7.56691E-06
STDEV	505321433	1.558013832	4.525474918	1.768101988

[Table 17]: A summary of the LOD of organics in Na_3PO_4 in M. The subsequent STDEV of the averaged 1000 trials is also listed. The STDEV of all values, except tryptophan, are within an order of magnitude from the LOD. Tryptophan STDEV can be attributed to the high level of variance between data points. Four out of the six points are outliers.

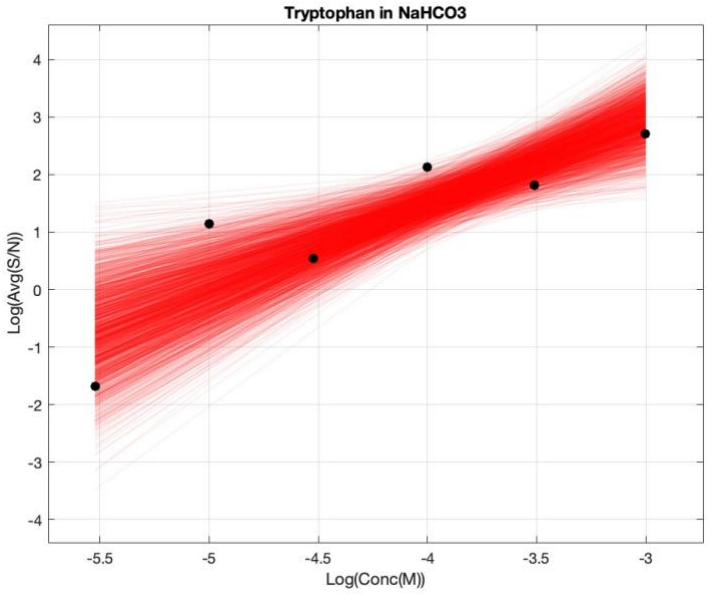

Figure 14: The Monte Carlo regression series, spanning 1000 iterations of the likely best fit according to STDEV of individual data points of tryptophan in sodium bicarbonate.

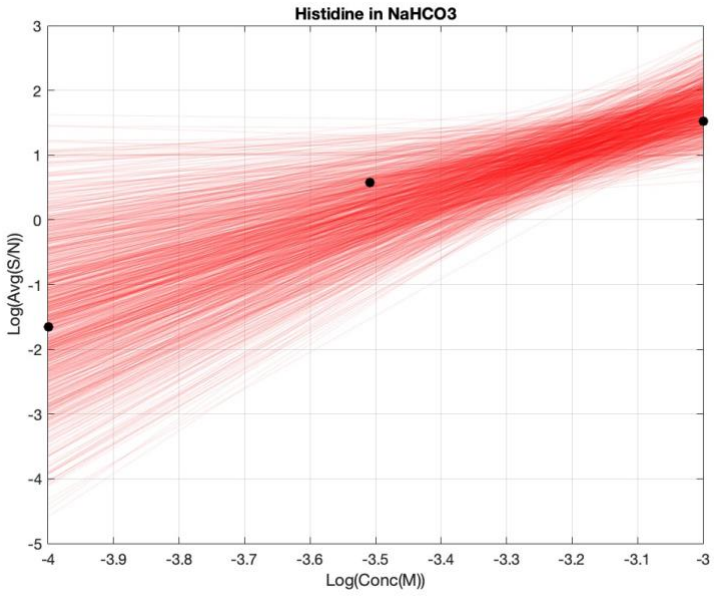

Figure 15: The Monte Carlo regression series, spanning 1000 iterations of the likely best fit according to STDEV of individual data points of histidine in sodium bicarbonate.

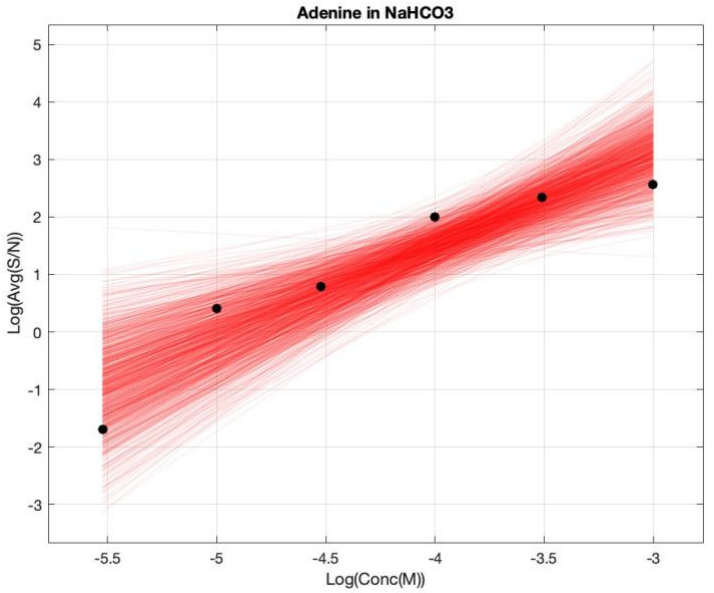

Figure 16: The Monte Carlo regression series, spanning 1000 iterations of the likely best fit according to STDEV of individual data points of adenine in sodium bicarbonate.

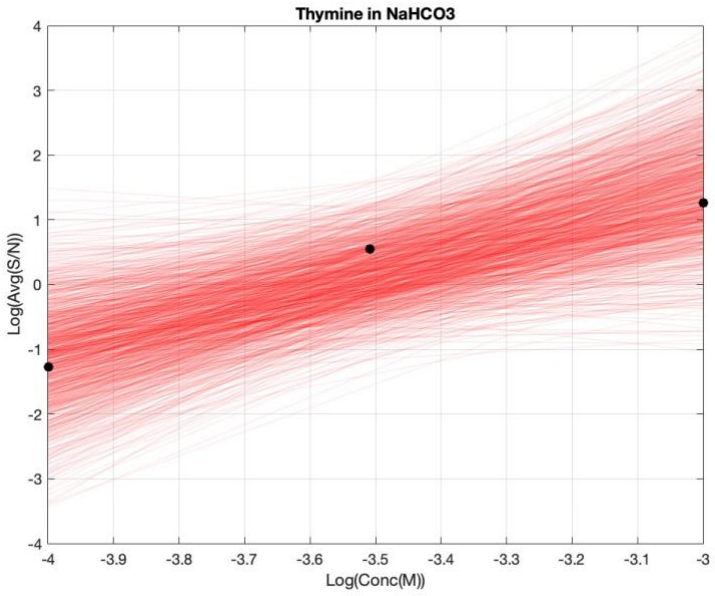

Figure 17: The Monte Carlo regression series, spanning 1000 iterations of the likely best fit according to STDEV of individual data points of thymine in sodium bicarbonate.

	Tryptophan	Histidine	Adenine	Thymine
LOD $NaHCO_3$	2.44413E-05	0.000439026	2.77223E-05	0.000548714
STDEV	2.319963911	4.599540269	2.154565253	537.3920173

[Table 18]: A summary of the LOD of organics in $NaHCO_3$ in M. The subsequent STDEV of the averaged 1000 trials is also listed. The STDEV was extremely high for thymine due to the lack of observable data points, whereas the other organics had errors within one order of magnitude.

Conclusion

With the composition of the matrix having a distinct effect on the LOD of organics via LDMS, we refute the null hypothesis that salt composition will not impact the detection limit of the organic analytes. By simulating salt compositions analogous to Enceladus' plumes, this research enhances our understanding of how salt matrices might influence the detectability of biosignatures such as amino acids and nucleobases. The ability of LDMS to detect and quantify complex organics by analyzing m/z peaks and S/N ratios underscores its applicability for spaceflight missions. LDMS instruments are currently baselined for the ExoMars rover (scheduled to launch on Mars in 2028; Goesmann et al., 2017), the Dragonfly mission to Titan (scheduled to launch in 2028; Li et al., 2023), and future Artemis missions (Ray et al., 2024). These efforts set the stage for LDMS to play a pivotal role in future Enceladus exploration missions by advancing the understanding of how mineralogy affects the ability to search for alien life, specifically on ocean worlds. Among the matrices tested, Na_3PO_4 consistently provided the lowest detection limits for most analytes, while $NaHCO_3$ showed the least favorable results. These advancements enhance LDMS methodologies for use in planetary exploration and provide valuable insights for interpreting data

from future missions. Ultimately, this research underscores the potential of LDMS as a powerful tool for probing the chemical complexity and habitability of ocean worlds like Enceladus.

References

Alterman, M. A., Gogichayeva, N. V., & Kornilayev, B. A. (2004). Matrix-assisted laser desorption/ionization time-of-flight mass spectrometry-based amino acid analysis. *Analytical Biochemistry*, *335*(2), 184–191. https://doi.org/10.1016/j.ab.2004.06.031

Antoine, R., & Dugourd, P. (2013). UV–Visible Absorption Spectroscopy of Protein Ions. In S. Brøndsted Nielsen & J. A. Wyer (Eds.), *Photophysics of Ionic Biochromophores* (pp. 141–153). Springer Berlin Heidelberg. https://doi.org/10.1007/978-3-642-40190-9_8

Arevalo, R., Willhite, L., Bardyn, A., Ni, Z., Ray, S., Southard, A., Danell, R., Grubisic, A., Gundersen, C., Minasola, N., Yu, A., Fahey, M., Hernandez, E., Briois, C., Thirkell, L., Colin, F., & Makarov, A. (2023). Laser desorption mass spectrometry with an Orbitrap analyser for in situ astrobiology. *Nature Astronomy*, *7*(3), 359–365. https://doi.org/10.1038/s41550-022-01866-x

Bada, & McDonald. (1995). Amino Acid Racemization on Mars: Implications for the Preservation of Biomolecules from an Extinct Martian Biota. *Icarus*, *114*(1), 139–143. https://doi.org/10.1006/icar.1995.1049

Cafferty, B. J., & Hud, N. V. (2014). Abiotic synthesis of RNA in water: A common goal of prebiotic chemistry and bottom-up synthetic biology. *Current Opinion in Chemical Biology*, *22*, 146–157. https://doi.org/10.1016/j.cbpa.2014.09.015

Cobb, A. K., & Pudritz, R. E. (2014). NATURE'S STARSHIPS. I. OBSERVED ABUNDANCES AND RELATIVE FREQUENCIES OF AMINO ACIDS IN METEORITES. *The Astrophysical Journal*, *783*(2), 140. https://doi.org/10.1088/0004-637X/783/2/140

Dair, G. T. (2001). Absorption of 193- and 213-nm Laser Wavelengths in Sodium Chloride Solution and Balanced Salt Solution. *Archives of Ophthalmology*, *119*(4), 533. https://doi.org/10.1001/archopht.119.4.533

Franchi, M. (2003). Cations as Mediators of the Adsorption of Nucleic Acids on Clay Surfaces in Prebiotic Environments. *Origins of Life and Evolution of the Biosphere*, *33*(1), 1–16. https://doi.org/10.1023/A:1023982008714

Guo, X., Fu, S., Ying, J., & Zhao, Y. (2023). Prebiotic chemistry: A review of nucleoside phosphorylation and polymerization. *Open Biology*, *13*(1), 220234. https://doi.org/10.1098/rsob.220234

Halmann, M., & Platzner, I. (1965). 254. The photochemistry of phosphorus compounds. Part II. Far-ultraviolet absorption spectra of some phosphorus oxyanions in aqueous solution. *Journal of the Chemical Society (Resumed)*, 1440. https://doi.org/10.1039/jr9650001440

Higgs, P. G., & Pudritz, R. E. (2009). A Thermodynamic Basis for Prebiotic Amino Acid Synthesis and the Nature of the First Genetic Code. *Astrobiology*, *9*(5), 483–490. https://doi.org/10.1089/ast.2008.0280

Jiménez-Serra, I., Martín-Pintado, J., Rivilla, V. M., Rodríguez-Almeida, L., Alonso Alonso, E. R., Zeng, S., Cocinero, E. J., Martín, S., Requena-Torres, M., Martín-Domenech, R., & Testi, L. (2020). Toward the RNA-World in the Interstellar Medium—Detection of Urea and Search of 2-Amino-oxazole and Simple Sugars. *Astrobiology*, *20*(9), 1048–1066. https://doi.org/10.1089/ast.2019.2125

Keller, G. (2017). *Electrical Properties of Rocks and Minerals* (Vol. 1).

Martins, Z. (2018). The Nitrogen Heterocycle Content of Meteorites and Their Significance for the Origin of Life. *Life*, *8*(3), 28. https://doi.org/10.3390/life8030028

Mavrikakis, M., Hammer, B., & Nørskov, J. K. (1998). Effect of Strain on the Reactivity of Metal Surfaces. *Physical Review Letters*, *81*(13), 2819–2822. https://doi.org/10.1103/PhysRevLett.81.2819

Mojarro, A., Ruvkun, G., Zuber, M. T., & Carr, C. E. (2017). Nucleic Acid Extraction from Synthetic Mars Analog Soils for *in situ* Life Detection. *Astrobiology*, *17*(8), 747–760. https://doi.org/10.1089/ast.2016.1535

National Academies of Sciences, Engineering. (2023). *Origins, Worlds, and Life: Planetary Science and Astrobiology in the Next Decade*. The National Academies Press. https://doi.org/10.17226/27209

Neveu, M., Anbar, A. D., Davila, A. F., Glavin, D. P., MacKenzie, S. M., Phillips-Lander, C. M., Sherwood, B., Takano, Y., Williams, P., & Yano, H. (2020). Returning Samples From Enceladus for Life Detection. *Frontiers in Astronomy and Space Sciences*, *7*, 26. https://doi.org/10.3389/fspas.2020.00026

Permyakov, E. A. (2012). The Use of UV–Vis Absorption Spectroscopy for Studies of Natively Disordered Proteins. In V. N. Uversky & A. K. Dunker (Eds.), *Intrinsically Disordered Protein Analysis* (Vol. 895, pp. 421–433). Humana Press. https://doi.org/10.1007/978-1-61779-927-3_24

Postberg, F., Kempf, S., Schmidt, J., Brilliantov, N., Beinsen, A., Abel, B., Buck, U., & Srama, R. (2009). Sodium salts in E-ring ice grains from an ocean below the surface of Enceladus. *Nature*, *459*(7250), 1098–1101. https://doi.org/10.1038/nature08046

Postberg, F., Khawaja, N., Abel, B., Choblet, G., Glein, C. R., Gudipati, M. S., Henderson, B. L., Hsu, H.-W., Kempf, S., Klenner, F., Moragas-Klostermeyer, G., Magee, B., Nölle, L., Perry, M., Reviol, R., Schmidt, J., Srama, R., Stolz, F., Tobie, G., … Waite, J. H. (2018).

Macromolecular organic compounds from the depths of Enceladus. *Nature*, *558*(7711), 564–568. https://doi.org/10.1038/s41586-018-0246-4

Postberg, F., Sekine, Y., Klenner, F., Glein, C. R., Zou, Z., Abel, B., Furuya, K., Hillier, J. K., Khawaja, N., Kempf, S., Noelle, L., Saito, T., Schmidt, J., Shibuya, T., Srama, R., & Tan, S. (2023). Detection of phosphates originating from Enceladus's ocean. *Nature*, *618*(7965), 489–493. https://doi.org/10.1038/s41586-023-05987-9

Scigelova, M., & Makarov, A. (2006). Orbitrap Mass Analyzer – Overview and Applications in Proteomics. *PROTEOMICS*, *6*(S2), 16–21. https://doi.org/10.1002/pmic.200600528

Self, D. E., & M. C. Plane, J. (2002). Absolute photolysis cross-sections for $NaHCO_3$, NaOH, NaO, NaO_2 and NaO_3: Implications for sodium chemistry in the upper mesosphere. *Phys. Chem. Chem. Phys.*, *4*(1), 16–23. https://doi.org/10.1039/B107078A

Snyder, L. E., Lovas, F. J., Hollis, J. M., Friedel, D. N., Jewell, P. R., Remijan, A., Ilyushin, V. V., Alekseev, E. A., & Dyubko, S. F. (2005). A Rigorous Attempt to Verify Interstellar Glycine. *The Astrophysical Journal*, *619*(2), 914–930. https://doi.org/10.1086/426677

Srama, R., Ahrens, T. J., Altobelli, N., Auer, S., Bradley, J. G., Burton, M., Dikarev, V. V., Economou, T., Fechtig, H., Görlich, M., Grande, M., Graps, A., Grün, E., Havnes, O., Helfert, S., Horanyi, M., Igenbergs, E., Jessberger, E. K., Johnson, T. V., … Zook, H. A. (2004). The Cassini Cosmic Dust Analyzer. *Space Science Reviews*, *114*(1–4), 465–518. https://doi.org/10.1007/s11214-004-1435-z

Tanaka, M., & Nagakura, S. (1966). Electronic structures and spectra of adenine and thymine. *Theoretica Chimica Acta*, *6*(4), 320–332. https://doi.org/10.1007/BF00537278

Tolstoguzov, V. (2004). Why Were Polysaccharides Necessary? *Origins of Life and Evolution of the Biosphere*, *34*(6), 571–597. https://doi.org/10.1023/B:ORIG.0000043127.18942.c4

Waite, J. H., Combi, M. R., Ip, W.-H., Cravens, T. E., McNutt, R. L., Kasprzak, W., Yelle, R., Luhmann, J., Niemann, H., Gell, D., Magee, B., Fletcher, G., Lunine, J., & Tseng, W.-L. (2006). Cassini Ion and Neutral Mass Spectrometer: Enceladus Plume Composition and Structure. *Science*, *311*(5766), 1419–1422. https://doi.org/10.1126/science.1121290